Characterization of robotized CMT-WAAM carbon steel

Tankova, Trayana; Andrade, David; Branco, Ricardo; Zhu, Carlos; Rodrigues, Dulce; Simões da Silva, Luís

DOI
10.1016/j.jcsr.2022.107624

Publication date
2022

Document Version
Final published version

Published in
Journal of Constructional Steel Research

Journal of Constructional Steel Research 199 (2022) 107624

Contents lists available at ScienceDirect

Journal of Constructional Steel Research

journal homepage: www.elsevier.com/locate/jcsr

Characterization of robotized CMT-WAAM carbon steel

Trayana Tankova [a,b,*], David Andrade [b], Ricardo Branco [c], Carlos Zhu [c], Dulce Rodrigues [b], Luís Simões da Silva [b]

[a] Delft University of Technology, Department of Engineering Structures, Netherlands
[b] University of Coimbra, ISISE, Department of Civil Engineering, Portugal
[c] University of Coimbra, CEMMPRE, Department of Mechanical Engineering, Portugal

ARTICLE INFO

Keywords:
Steel
WAAM
Additive manufacturing
Material properties
Carbon steel

ABSTRACT

This paper analyses the microstructural and mechanical properties of carbon steel coupons produced by CMT-WAAM. The strategy adopted in the fabrication of the test specimens using a robotised facility is explained. Then, the results of the mechanical characterization performed using as-built and machined samples, extracted in several directions (0°, 45°, 90°) relative to the material deposition trajectory, are analysed. The yield and ultimate tensile strengths were determined by performing tensile tests and the Young's modulus was determined using ultra-micro hardness measurements. A deep microstructural characterization was also performed by optical microscopy for establishing a direct relationship between the manufacturing procedures and the registered mechanical properties. The failure micro-mechanisms associated with the building orientation and the surface condition was also examined by scanning electron microscopy. It was found out that the additive manufactured material has isotropic tensile properties, which result from the formation of an annealed microstructure upon cooling from the successive CMT-WAAM thermal cycles. The machined specimens exhibit higher strength and ductility than the as-built ones. The fracture surfaces of both machined and as-built coupons showed ductile failure. The results of the uniaxial tensile tests indicate that the machined and as-built WAAM steel walls satisfy the requirements of a structural steel grade as specified by Eurocode 3.

1. Introduction

Steel is one of the most versatile materials, available in different forms such as sections, rebars and plates. Its applications range from construction to automotive and aerospace. Being a crucial ingredient of the built environment, steel exists in almost every building and infrastructure. Although steel exists for over 150 years and remains the backbone of modern civilisation, most steels used today did not exist 20 years ago, according to the *worldsteel* association. Furthermore, the steel production, fabrication and erection are highly standardized. The steel product standards (i.e. EN10025 [1]), for example, are linked to the execution standards (i.e. EN1090 [2]) and design standards (i.e. EN1993 [3]).

As an alternative to the conventional steel fabrication processes, additive manufacturing (AM) of steel is rapidly gaining popularity due to the free-form capabilities and the possibility to combine several materials into one product. Metals, in general, can be processed through different AM methods [4]. Among them, the most suitable for large scale parts, in terms of speed and layout, is a directed energy deposition (DED) method, named wire and arc additive manufacturing (WAAM). However, besides its advantages, WAAM presents a major challenge, as the final material and geometrical properties are determined by the manufacturing procedures and parameters that need to be optimized case by case. The WAAM fabricated parts undergo fast cooling, which may result in internal defects and/or non-homogeneous material properties, with important influence on the strength and stiffness of the final component, as well as the formation of residual stresses and distortions [5]. These phenomena are induced by the process related thermal cycles, being determined by the maximum temperatures attained during the manufacturing and by the cooling rates, which in turn are determined by the manufacturing procedures/trajectory and process parameters [6].

There are several techniques for the improvement of the material properties, such as the optimisation of the trajectory, the control of the heating and/or cooling cycles and, in some cases, the use of post-processing techniques such as heat treatment or cold rolling [7–9]. However, before applying any post-manufacturing technique, it is

* Corresponding author at: Delft University of Technology, Civil Engineering & Geosciences, Stevinweg 1, 2628 CN Delft, Netherlands.
E-mail address: t.tankova@tudelft.nl (T. Tankova).

https://doi.org/10.1016/j.jcsr.2022.107624
Received 28 June 2022; Received in revised form 7 October 2022; Accepted 12 October 2022
Available online 27 October 2022

important to establish the link between the process parameters and the resulting material properties as a starting point for future improvements.

Although WAAM material properties are not yet sufficiently well characterized, there are a few studies on their characterization. They cover different wire materials and welding parameters. There is a group of studies that covers the behaviour of carbon steel material ER70S-6 [14–23]. They focused on various aspects such as coupon tests with different orientations with respect to the printing direction for material deposited in layers or point-by-point, surface roughness and its influence on the strength, micro structural comparison between machined and non-machined coupons as well as proposals for models that describe the material behaviour of WAAM carbon steel.

In recent studies, several authors [15–17,24–26] characterized the microstructure of WAAM mild carbon steels and observed a non-homogeneous microstructure throughout the volume of the manufactured component. Due to the layer-by-layer nature of the WAAM process, and depending on the steels carbon content, alloying elements, process heat input and cooling rates, different lamellar microstructures varying from the top to the bottom of the manufactured parts have been reported. This could lead to anisotropic mechanical properties. For instance, Sridharan et al. [25] performed a microstructural and mechanical analysis on WAAM specimens produced with the ER-70S6 filler wire using a TIG welding system and observed significant scatter in tensile ductility and Charpy toughness results. In addition, Rafieazad et al. [15] also performed a microstructural and mechanical analysis on a wall manufactured by WAAM with the ER70S-6 wire using GMAW equipment. Similarly, it was observed that the plastic tensile strain at failure along the horizontal direction was three times larger than that in the vertical direction. Aldalur et al. [17] compared the influence of different deposition strategies on the microstructural and mechanical properties of the WAAM carbon steel components. In addition to the anisotropy of the mechanical properties, Silvestru et al. [23] also reported a strong influence of the printing direction on the geometry of bars produced using a Fronius 60i Robacta Drive Cold Metal Transfer (CMT) torch.

Contrary to what was reported by the previous studies, some authors [18–21,27] reported isotropic behaviour on the mechanical properties of the manufactured components, i.e. the influence of the sample orientation on the mechanical properties was negligible. Huang et al. [21], who performed a mechanical and microstructural analysis on WAAM walls produced with mild and high strength steels using a metal inert gas welding system, stated that the isotropic properties were related to the observed weak crystallographic texture. Furthermore, in the work performed by Al-Nabulsi et al. [22], it was also shown that the mechanical properties of WAAM components produced with the Union K 40 filler material using a GMAW equipment fulfil the requirements for a structural steel grade for building structures as specified by part 1–1 of Eurocode 3 [3].

In [28–30], it is also mentioned that due to the influence of the thermal histories in the direction and shape of the grains, using additive manufacturing processes with low heat input, such as WAAM CMT (CMTAW), may be beneficial for obtaining components with a more uniform microstructure and mechanical properties. Nevertheless, very few studies have examined, in a systematic way, the microstructural features and the mechanical behaviour of carbon steel produced by CMTAW. Nagasai et al. [14] investigated the effect of the heat input on the microstructural and mechanical properties of carbon steel cylindrical components produced by GMAW and CMTAW processes. Due to the lower heat input induced by the CMTAW process, the parts produced by this technique had smaller grain size and higher mechanical strength. However, the GMAW and CMTAW cylindrical components showed anisotropic tensile properties. Another unclear aspect is the benefit in terms of mechanical behaviour of having machined surfaces when compared to an as-built condition. This paper analyses the microstructural and mechanical properties of carbon steel parts, in machined and as-built conditions, produced by WAAM using the CMT technique. Firstly, the fabrication of the test specimens using a robotised WAAM facility is explained. Then, the results of the mechanical characterization performed using samples extracted in several directions (0°, 45°, 90°) relative to the material deposition trajectories are analysed. The yield and ultimate tensile strengths were determined by performing tensile tests and the Young's modulus was determined using ultra-micro hardness measurements. A deep microstructural characterization was also performed for establishing a direct relationship between the manufacturing procedures and the registered mechanical properties. The failure micro-mechanisms associated with the different building directions and surface conditions were also examined by scanning electron microscopy.

2. Experimental programme

2.1. Fabrication of test specimens

Specimens were fabricated at the Additive Manufacturing Laboratory of the University of Coimbra [10] which is equipped with an ABB IRB 4600 robot and a CMT welding machine Fronius TPS 400i. For research purposes, a wall with dimensions 500 × 300 × 8 mm was produced (Fig. 1). The welding parameters, which are given in Table 1, were defined in order to ensure an optimum productivity from a perspective of a robotic-based system. The fabrication process took about 4 h without interruptions besides the estimated cooling time between the successive deposition of layers.

The chosen deposition strategy is shown in Fig. 2, whereby a rectangular perimeter, with a single line infill, was adopted. In each layer, the perimeter was printed and then the infill was deposited. To avoid defects associated with the accumulation of material, the starting point for the successive layers was random.

The feedstock material used was welding wire ER70S-6, with copper coating, 1 mm diameter and 98% Ar + 2% CO_2 (M12) shielding gas. The shielding gas definitions were also set to ensure an optimum productivity from the perspective of a robotic-based system. Table 2 and Table 3 summarize the chemical composition and the mechanical properties of the as-welded feedstock material, as provided by the manufacturer.

2.2. Mechanical and microstructural characterization

Tensile tests were carried out according to ISO 6892 [11]. A total of 18 coupons were milled from the WAAM steel wall, according to the sampling directions shown in Fig. 3 a: vertical (0°), inclined (45°) and horizontal (90°). For each sampling direction, half of the samples were machined, for smoothing the surface, and the other half were tested in

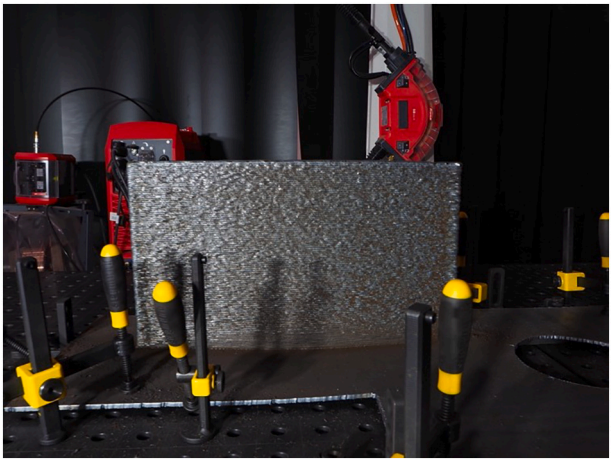

Fig. 1. WAAM wall.

Table 1
Welding parameters.

Current	Voltage	Wire feed	Robot speed
155 A	15.7 V	6 m/min	10 mm/s

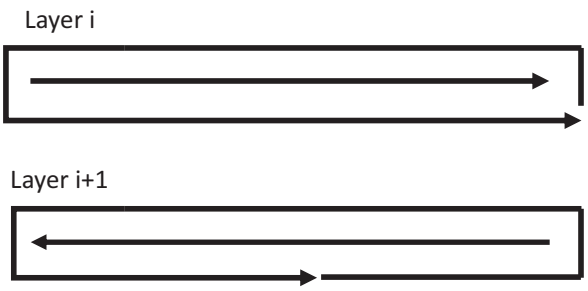

Fig. 2. Deposition strategy.

the as-built surface condition. The coupon dimensions are represented Fig. 3 b. The tests were performed in a Universal Machine W + B LFV 600kN, at room temperature in quasi-static loading conditions, using a mechanical extensometer Epsilon model 3542-025 M-050-ST. Due to the corrugated morphology of the as-built coupons, the stress-strain curves were calculated based on their average cross-sectional area, determined for its entire gauge length.

After the completion of the uniaxial tensile tests, the fracture surfaces of the tested specimens were examined using a Carl-Zeiss Gemini 500 FE-SEM scanning electron microscope (SEM), for comparing the main failure modes associated with the different testing conditions. Before examination, the samples were cut in a direction perpendicular to the longitudinal axis of the specimen with a high-speed cutting machine and then were ultrasonically cleaned in trichloroethylene solution for ten minutes.

Hardness measurements were performed in different locations and orientations of the wall, including the bottom, middle and top zones, along the longitudinal (LD), transverse (TD) and normal (ND) directions (Fig. 3), using a Shimadzu Microhardness Tester, with 200 g load and 15 s holding time. In addition, to complement the mechanical characterization of the manufactured wall, the Young's modulus was determined through depth-sensing ultra-micro-indentation using a Fisherscope H100 equipment, following the methodology proposed in Oliver and Pharr [12]. The indentation tests were carried out at 500 mN peak load with 60 s of loading time, 30 s of holding at the peak load and 60 s of unloading. The Young's modulus results were obtained by averaging 15 indentations all over the wall.

Finally, for the microstructural analysis, metallographic samples were extracted from the wall along the LD, TD and ND directions, polished according to standard procedures up to 1 μm surface finish, etched with 2% Nital and observed using an optical microscope (Leica DM 4000 M LED).

3. Results & discussion

3.1. Mechanical properties

The stress-strain curves of the 0°, 45° and 90° samples, tested in the machined and as-built conditions, are shown in Fig. 4. The averages of the maximum and the minimum values of the yield strength (f_y), ultimate tensile strength (f_u) and fracture strain (ε_f), for each type of tested sample, were determined and they are summarized in the bar chart in Fig. 5 and Table 4 for the as-built and machined samples. Analysing Fig. 4, it is possible to conclude that all the machined and as-built coupons exhibited the stress-strain behaviour typical of hot-rolled structural carbon steels. The linear elastic region and the yielding plateau, common to these steels, are well discernible in all the curves, as well as the strain hardening region, followed by the necking stage before failure. Although the yielding plateau can be easily identified in the curves corresponding to the machined and as-built samples, its size is larger and more uniform for the machined samples. As it is well-known, the formation of the Lüders bands, responsible for the yielding plateau, may be affected by the macroscopic geometry of the test coupons [13]. Hence, the differences in the size and shape of the yield plateau between the machined and as-built parts indicate that the deformation, at the onset of the plastic deformation, was more uniform for the machined samples.

It is also possible to conclude that despite the similarities in the evolution of the stress-strain curves, in the plastic domain, the engineering stress and strain values were always higher for the machined coupons, independently of the orientation of the sample, as shown in Fig. 5. According to the figure, the average f_y, f_u and ε_f values, for all orientations of the samples, were equal to 320 MPa, 444 MPa and 27%, for the as-built samples, and equal to 378 MPa, 504 MPa and 37%, for the machined samples. This shows that the machining operation led to an increase of 18%, 14% and 39% of the average f_y, f_u and ε_f values, respectively.

Comparing the stress-strain curves for the 0°, 45° and 90° coupons, it is possible to conclude that, in general, there was a good reproducibility of the results obtained for both the machined and as-built samples. For the 0°, 45° and 90° as-built samples, the average f_y values were equal to

Table 3
Mechanical properties of the feedstock material (ER70S-6).

Feedstock wire	*Yield Stress [MPa]*	*Ultimate tensile strength [MPa]*
ER70S-6	420	520

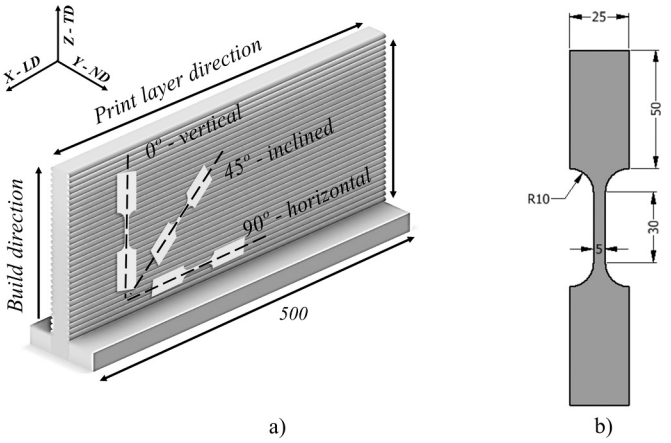

Fig. 3. (a) Schematic representation of the printed wall and orientations of the extracted tensile coupons (vertical – 0°, inclined - 45°, horizontal – 90°). (b) Standard tensile coupon geometry (units: millimetres).

Table 2
Chemical composition of the ER70S-6 feedstock wire (wt%).

Feedstock wire	*C*	*Mn*	Cr	Ni	Mo	V	P	Fe
ER70S-6	0.05–0.15	1.40–1.85	0.15 max	0.15 max	0.15 max	0.03 max	0.025 max	Bal.

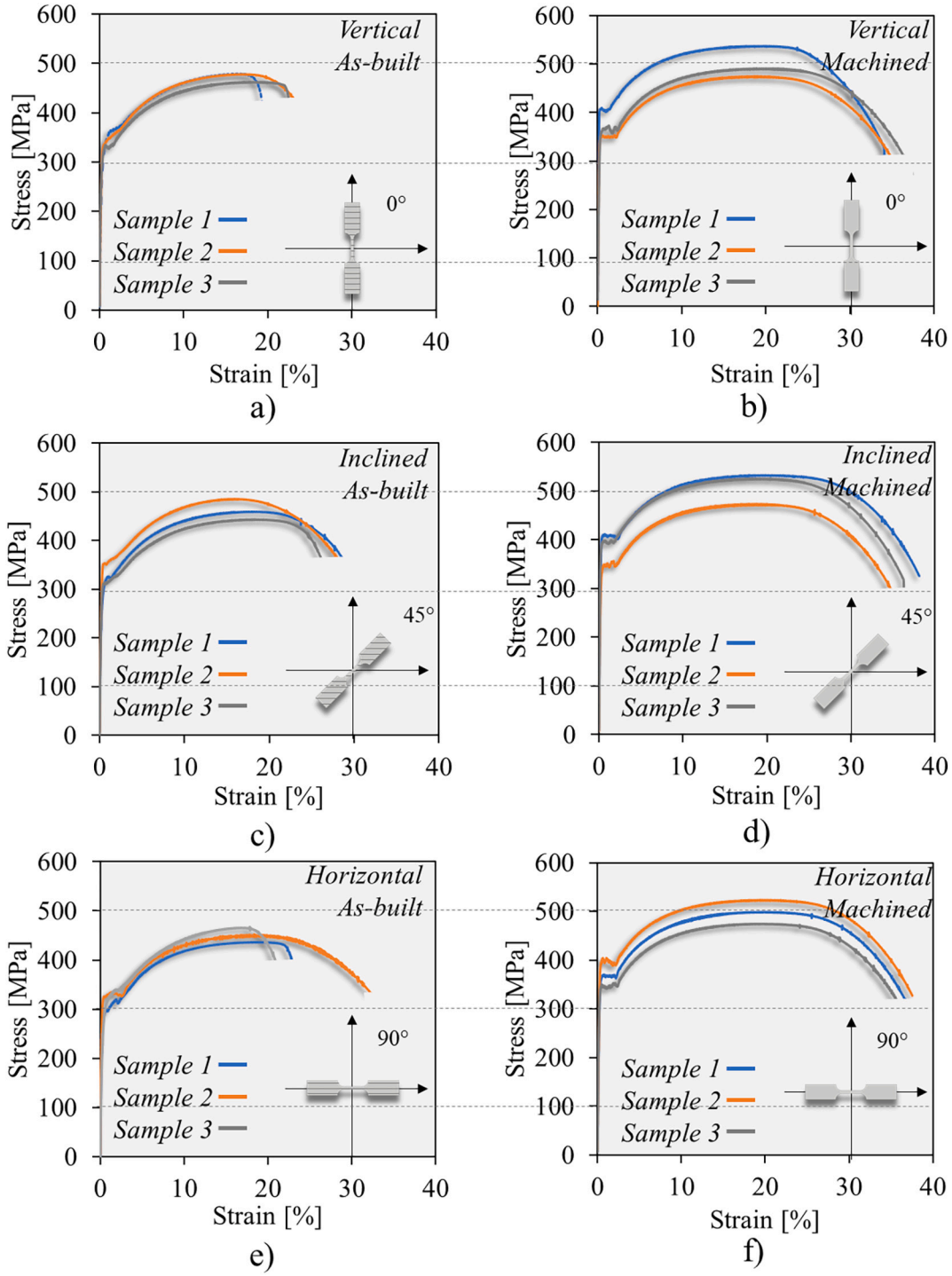

Fig. 4. Stress-strain curves for the (a, c and e) as-built and (b, d and f) machined coupons with various orientations: 0°(vertical), 45° (inclined) and 90°(horizontal), relative to the print layer direction.

336 MPa, 319 MPa and 304 MPa, with a maximum and minimum deviation of ±6.1%, ± 5.8% and ± 4%, respectively, while the average f_u values were equal to 457 MPa, 442 MPa and 432 MPa, with a maximum and minimum deviation of ±0.5%, ± 3.9% and ± 3.1%, respectively. A similar trend was observed for the machined samples, for which the average f_y values for the 0°, 45° and 90° orientations were equal to 376 MPa, 384 MPa and 373 MPa, with a maximum and minimum deviation of ±8.3%, 8.9% and 7.6%, respectively, while the average f_u values were equal to 502 MPa, 511 MPa and 499 MPa, with a maximum and minimum deviation of ±6.3%, 6.2% and 5.0%, respectively. The tensile test results clearly show the isotropy in mechanical properties of the manufactured wall, i.e. the negligible influence of the tensile samples orientation on the mechanical properties of the wall. In fact, for the as-built samples, varying the orientation from 0° to 90° resulted in a variation of 10% and 5% for the f_y, and f_u values, respectively. In comparison, for the machined samples, varying the tensile samples orientation resulted in a variation of 2.7% and 2.4% on the f_y, and f_u values, respectively. However, this difference is not necessarily attributed to the sample orientation but rather on the type of defects that may exist in the different directions.

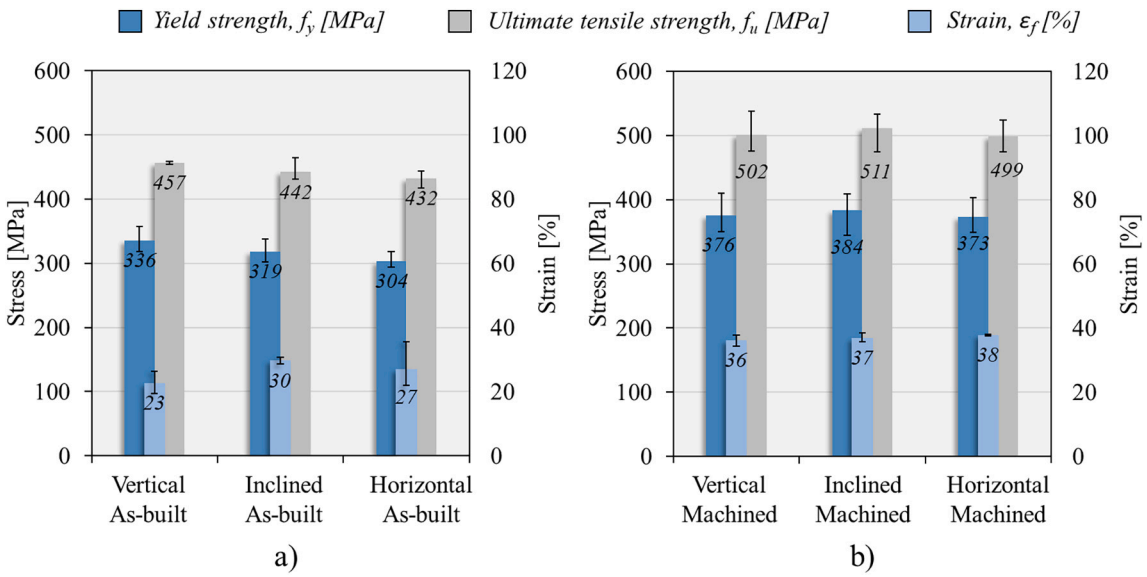

Fig. 5. Average, minimum and maximum material properties (yield strength, ultimate tensile strength and failure strain) for the (a) as-built and (b) machined coupons with various orientations: 0°(vertical), 45° (inclined) and 90°(horizontal).

Table 4
Average values of the measured mechanical properties.

	Machined			As-built		
Test	Vertical (90°)	Inclined (45°)	Horizontal (0°)	Vertical (90°)	Inclined (45°)	Horizontal (0°)
f_y [MPa]	375.7	383.7	373.2	335.8	318.7	303.8
f_u [MPa]	501.5	511.8	499.3	462.6	447.0	428.2
f_u / f_y	1.33	1.33	1.34	1.38	1.40	1.41
ε_f [%]	36.2	36.9	37.8	22.8	29.8	27.0
ε_u [%]	19.2	18.2	19.3	17.1	17.4	18.3
15 ε_y [%]	2.36	2.34	2.77	2.66	2.78	2.71
E [GPa]	237.1	245.7	202.1	189.1	171.8	168.2

The only exception in terms of the uniformity in mechanical properties is related to the fracture strains of the as-built samples, with average ε_f values equal to 23%, 30% and 27%, for the 0°, 45° and 90° samples, respectively. For each direction tested, i.e. for the 0°, 45° and 90° samples, a maximum and minimum deviation of ±16.3%, 3.5% and 27.3% for the 0°, 45° and 90° samples, respectively, was observed. The scatter in ε_f is related to the varying thickness in the necking region, for the different as-built samples, but also the influence of surface defects which may lead to premature failure; this is further addressed in section 3.3. This is also evidenced by the fact that the strain values at failure, for the machined samples, with smooth surface finish, present more uniform values than those obtained for the as-built samples, i.e., the ε_f maximum e minimum deviation values for the machined samples were equal to ±5%, 3.8% and 0.7% for the 0°, 45° and 90° samples, respectively.

Furthermore, according to Eurocode 3, part 1–1, the structural steels should comply with ductility requirements (clause 3.2.2 (1)) which involve the ratio between the tensile strength and the yield stress, elongation at failure and ratio between strain at tensile stress and yield strain, as summarized in Eq. (1–3.)

$$\frac{f_u}{f_y} > 1.1 \tag{1}$$

$$\varepsilon_f > 15\% \tag{2}$$

$$\varepsilon_u > 15\varepsilon_y \tag{3}$$

The ratio between the tensile strength f_u and the yield stress f_y is given for the machined and as-built coupons in Table 4. It is satisfied for both the machined and as-built coupons, where even higher ratios are found for the as-built material. The strain criteria also satisfy the limits of Eqs. (2) and (3).

The modulus of elasticity was estimated from the stress-strain curves, where higher values were found for the machined coupons in the vertical and inclined directions. However, since there is no standardized procedure for the estimation of the modulus of elasticity from a standard coupon test, the result may not be reliable. Further analysis of the material hardness is used for a more realistic estimation of the young's modulus in section 3.4.

Finally, comparing the mechanical properties (average f_y, f_u and ε_f values) of the as-welded samples with the machined samples, provided in Table 4, it is possible to conclude that the mechanical strength of the deposited material resembles steel grade S355, whereas the as-built samples with their decrease in strength are closer to S275.

Fig. 6 compares the average, maximum and minimum values of f_y, f_u and ε_f obtained in the current work with the mechanical properties of WAAM mild carbon steels components reported by other authors in [14–23]. The figure shows the results of works that used several types of feedstock wire, such as the ER70S-6, ER110S-G and K 40, with a corresponding equivalent carbon content of 0.25–0.49%, 0.66% and 0.28%, respectively, and two different techniques, GMAW and CMT, represented in the figure by columns with solid and dashed edges, respectively. Furthermore, in the figure, it is also represented the surface finish of the tensile test specimens, i.e., if the coupons were tested in the as-built condition, the results are represented by columns filled with lines, whereas if the coupons were tested in machined condition, the results are represented by columns with a solid fill.

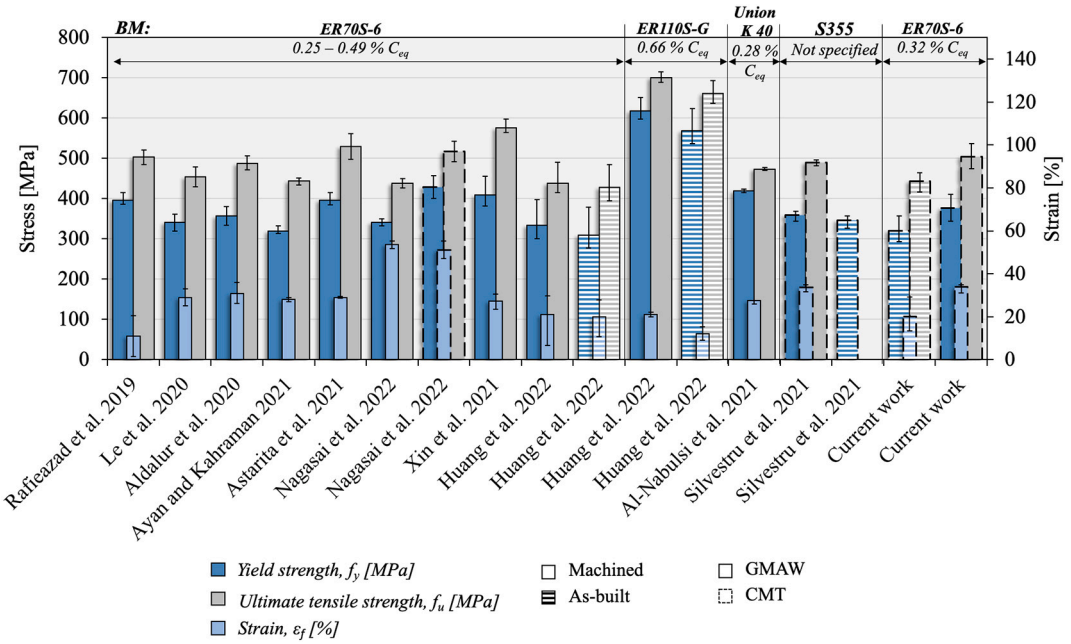

Fig. 6. Range of yield strength, ultimate tensile strength and fracture strain values for WAAM components reported in the literature in mild carbon steel.

From Fig. 6, it is possible to conclude that most of the published works used the GMAW process, with the ER70S-6 feedstock wire, for producing the WAAM parts, since this wire is one of the most common filler materials used to weld carbon steels. Another important conclusion is that most of the works considered in Fig. 6 only assessed the mechanical properties of machined coupons. The figure also shows that the range of mechanical properties obtained in the current work are in the range of those obtained by the other authors, even when comparing the as-built samples results with machined samples results. In fact, in addition to the present work, only Huang et al. [21] and Silvestru et al. [23] compared the mechanical properties of as-built and machined coupons, having concluded that, in agreement with the current results, the as-built samples always display lower mechanical properties than the machined ones, due to the stress concentrations associated with the rough surface of the as-built samples.

For structural applications, WAAM steels must satisfy Eurocode 3, part 1–1 material requirements for the minimum values of f_y and f_u. Currently, these steels are not covered by the standard and there is no product standard dealing with these steels. Nevertheless, Fig. 6 shows that there is a good correlation between the mechanical properties of the feedstock material, ER70S-6 (see Table 3) that satisfies the minimum requirements for f_y and f_u for S355 and the corresponding properties for the machined samples. The as-built coupons exhibit lower average values for f_y and f_u. Similar conclusions were also presented by Huang et al. [21], which shows that further investigation focusing on improving the surface finish of parts obtained by WAAM should be addressed in the future, to enhance the mechanical properties of the as-built components. Moreover, as shown by Huang et al. [21], who compared the mechanical properties of WAAM components produced by two different feedstock wires, another possible solution to improve the mechanical properties of the as-built components is to use wires with higher carbon content and, consequently, higher mechanical properties. Nevertheless, special attention must be given to preventing the printing of parts with very low ductility, due to the formation of brittle phases, such as martensitic and bainitic microstructures, or even due to the formation of defects induced by cold cracking.

3.2. Geometry of the test samples

The more uniform deformation observed at the yielding plateau for the machined samples may be related to the WAAM parts surface properties, which are characterized by a rough surface finishing. The rough surface finishing determines small variations of the samples cross-section area, along the gauge length, which work as stress concentrators during the tensile loading. The as-built surface quality may be assessed based on Fig. 7, where the results of the surface waviness measurements are illustrated. More precisely, Fig. 7 a presents a sketch of the as-built wall, which indicates the locations from where the samples shown in Fig. 7 b to d were extracted. The samples analysed correspond to the top (Fig. 7 b), middle (Fig. 7 c) and bottom (Fig. 7 d) regions of the wall, in the as-built condition, and Fig. 7 e relates to a machined sample. Analysing the figure, it is possible to conclude that the as-built wall shows a rough surface with some bulges caused by weld geometry and excess of temperature. The colour maps introduced on the edges of the as-built samples show the local thickness evolution along the height of the sample. Histograms of the wall thickness at the top, middle and bottom regions are also shown in Fig. 8. The histograms show that the wall thickness varied from a maximum of 11 mm, in a very localised region near the substrate, decreasing progressively with the wall height, up to a minimum thickness value of 6 mm, at the top of the wall. The average thickness values of the wall at the bottom, middle and top regions were equal to 9.7 mm, 7.9 mm and 7.1 mm, while the standard deviation values of these same zones are ±0.77 mm, ± 0.36 mm and 0.43 mm, respectively. The higher thickness was observed in the region near the substrate due to gravity effects. This was also reported in [31].

3.3. Analysis of the fracture surfaces

To better understand the differences in ductility between the as-built and machined samples, Fig. 9 shows the tensile tests fracture surfaces obtained by SEM, which illustrate the failure mechanisms and the morphological features for different samples. More precisely, Fig. 9 a to c shows the fracture morphology of 0°, 45° and 90° machined tensile specimens, respectively, and Fig. 9 d shows the fracture morphology of a 90° as-built sample. Analysing the figure, it is possible to conclude that the macroscopic fracture surface, for all the samples, displays the common features characteristic of ductile fracture. Moreover, the figure also shows that the machined samples (Fig. 9 a to c) exhibit smaller cross-sectional areas, in the necking region, than the as-built samples (Fig. 9 d), which corresponds to a more ductile behaviour at the onset of

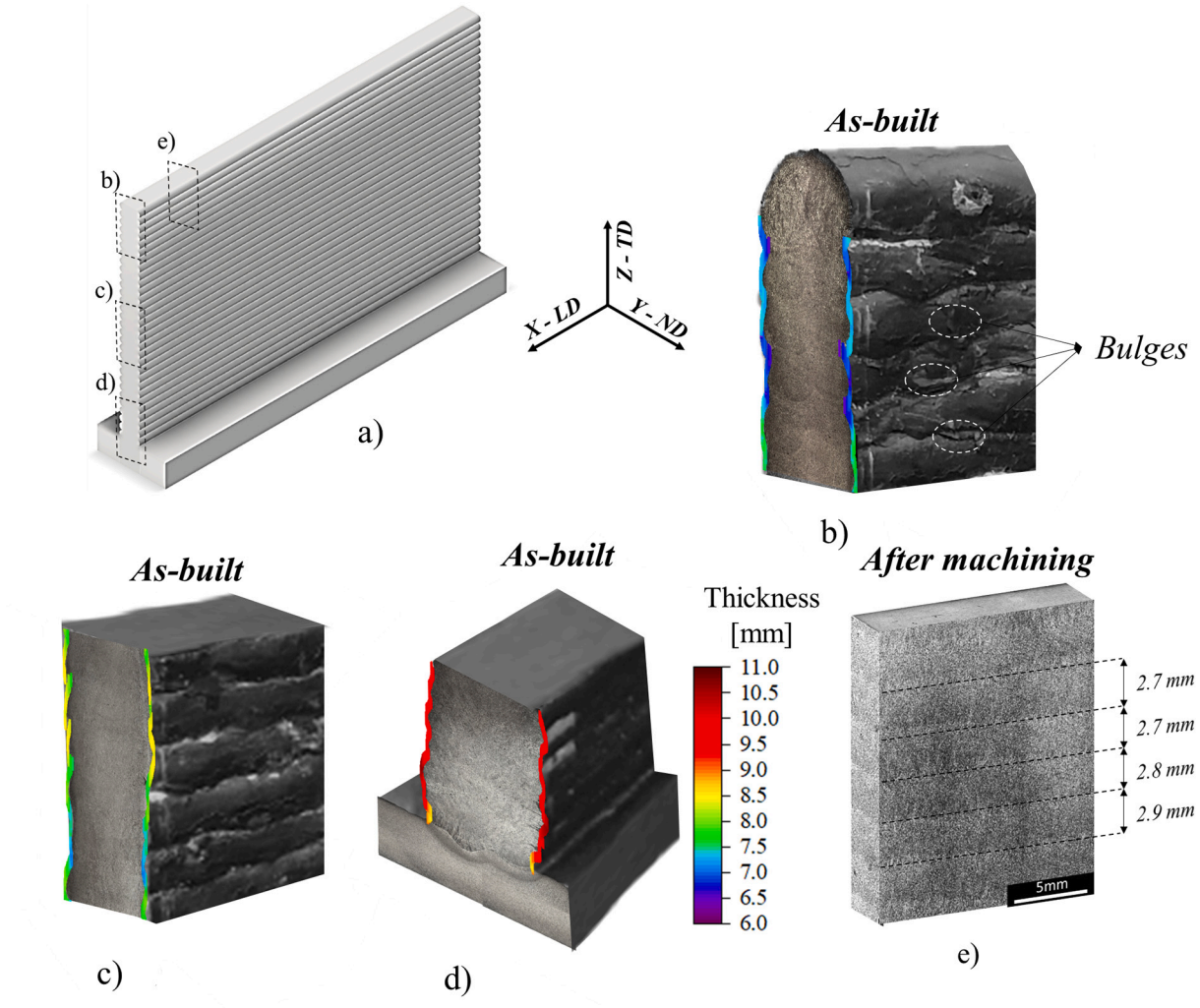

Fig. 7. (a) Wall geometry: in the as-built condition at the (b) top, (c) middle and (d) bottom wall zones a©(e) after the machining operation.

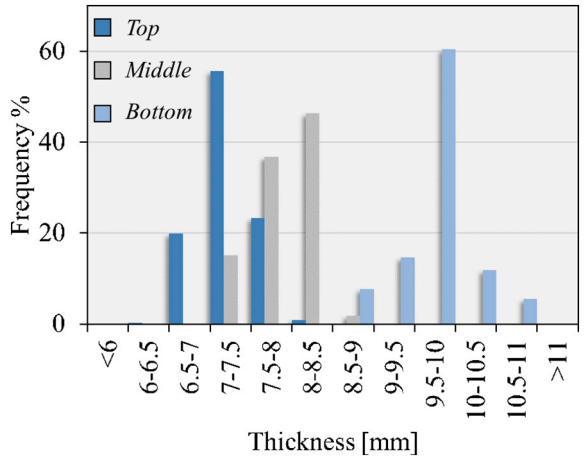

Fig. 8. Histograms of the as-built wall thickness distribution at the top, middle and bottom wall regions.

fracture. The lower ductility at the onset of fracture may explain the lower elongation calculated for the as-built specimens when analysing the tensile test results (Table 4).

The examination of the fracture surfaces in Fig. 9 also allows to identify a cup-and-cone shaped failure, with two distinct morphologic regions: a more fibrous region in the centre of the samples (magnified in Fig. 10), surrounded by a smoother region with 45° shear lips in the edges (magnified in Fig. 11). As can be seen in the magnified micrographs in Fig. 10, the central region exhibits equiaxed dimples, i.e. spherical depressions that coalesced normal to the loading axis, while in Fig. 11 it is possible to observe more elongated dimples with elliptical shapes, i.e. parabolic-like depressions that coalesced in planes of maximum shear stress. The same fracture behaviour has been reported by Nagasai et al. [14] and Chen et al. [32], respectively, for carbon steel and stainless steel WAAM samples after tensile loading. Fig. 12 a to d shows a more detailed analysis of the fibrous regions at high magnification for the machined (0°, 45° and 90°) and the as-built (90°) conditions. The figure reveals that the size and shape of the dimples were similar for the machined samples independently of the printing direction. Moreover, regarding the as-built samples, the conclusions were similar, but the fracture surfaces contained less dimples and exhibited some nearly flat regions (Fig. 12 d) not visible for the machined samples [14,16]. Rafieazad et al. [15] related the population of dimples with the ductility in low-carbon steel manufactured by WAAM. The authors advocated that in the material with higher ductility, deep dimples with uniform size and elongated shape are formed, which is also confirmed in the present study.

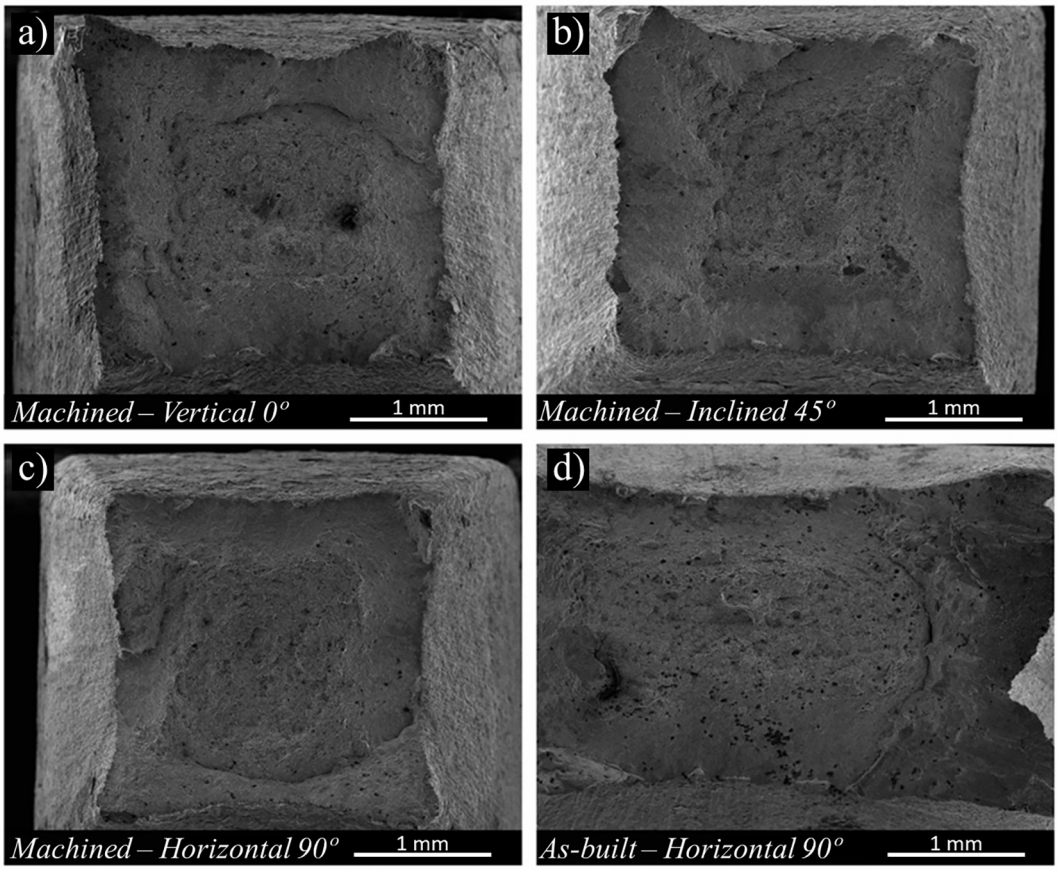

Fig. 9. Fracture morphology of tensile specimens at low magnification: (a) vertical, machined condition; (b) inclined, machined condition; (c) horizontal, machined condition; (d) horizontal, as-built condition.

3.4. Hardness study

The Young's Modulus and the hardness (H) evolution, in different directions of the wall, were also determined, using the depth-sensing indentation technique and microhardness testing, respectively. The Young Modulus results are shown in Fig. 13. Fig. 13 a exemplifies depth-sensing indentation load-displacement curves corresponding to the minimum (curve 1) and maximum hardness (curve 2) values recorded among all the measurements performed. The load-displacement curves show that the penetration depth was higher for curve 1, which corresponds to the region where the minimum hardness value was registered (150 $HV_{0.2}$), while the minimum penetration depth was registered for curve 2, which in turn, corresponds to the region where the maximum hardness value was registered (230 $HV_{0.2}$).

Analysing the unloading part of the load-displacement curves, the Young's modulus may be determined using the relationship [12],

$$\frac{1}{E_r} = \frac{1-\nu^2}{E} + \frac{1-\nu_i^2}{E_i}, \tag{4}$$

where E_r is the reduced Young's modulus, E_i (1140 GPa) and ν_i (0.07) are the Young's modulus and the Poisson's ratio of the diamond indenter tip, and ν is the Poisson's ratio of the deposited material which was considered equal to 0.3 as determined by [21] for ER70S-6 WAAM fabricated walls. Fig. 13 b shows a bar chart with the average, maximum and minimum Young's modulus and hardness ($HV_{0.2}$) values registered all over the deposited wall. Analysing the figure, it is possible to conclude that the average, maximum and minimum Young's modulus were equal to 214 GPa, 227 GPa and 202 GPa, respectively, which fell within the typical range values for conventional steels [16]. On the other hand, the average, maximum and minimum hardness values were equal to 192 $HV_{0.2}$, 230 $HV_{0.2}$ and 150 $HV_{0.2}$, respectively. According to these results, the Young's modulus and the hardness values varied around ±6% and ±24% throughout the wall geometry, showing that while the Young's modulus is an intrinsic property of a material related to the bond strength between atoms, the hardness' values may slightly vary according to the deposited material chemical composition and microstructure, which in turn depend on the cooling rates during deposition. In fact, the slight variation observed in Fig. 5, in the mechanical properties of the specimens tested in the same direction, may be related to the varying local hardness, since, as it is well known, there is a linear correlation between the steel hardness and the yield and ultimate tensile strengths [33].

3.5. Morphological and microstructural characterization

Fig. 14 shows optical micrographs representing the microstructural evolution from the bottom to the top of the wall, i.e. micrographs taken from the regions signalised in the bottom view macrograph of Fig. 14 a are shown in Fig. 14 d to g, micrographs taken from the regions signalised in the middle view macrograph of Fig. 14 b are shown in Fig. 14 h and i and micrographs taken from the regions signalised in the top view macrograph of Fig. 14 c are shown in Fig. 14 j and l. The micrograph of the substrate (Fig. 14 g) shows a ferritic–pearlitic microstructure with some banded patterns aligned with the steel rolling direction, which results from fluctuations in the concentration of alloying elements, such as manganese, across the plate thickness, due to the micro-segregation associated with the solidification stage during the production of the plates. The heating associated with the material deposition led to the formation of heat affected zone (HAZ) with an approximated penetration depth of 2 mm in the substrate, which is identified in Fig. 14 a. A

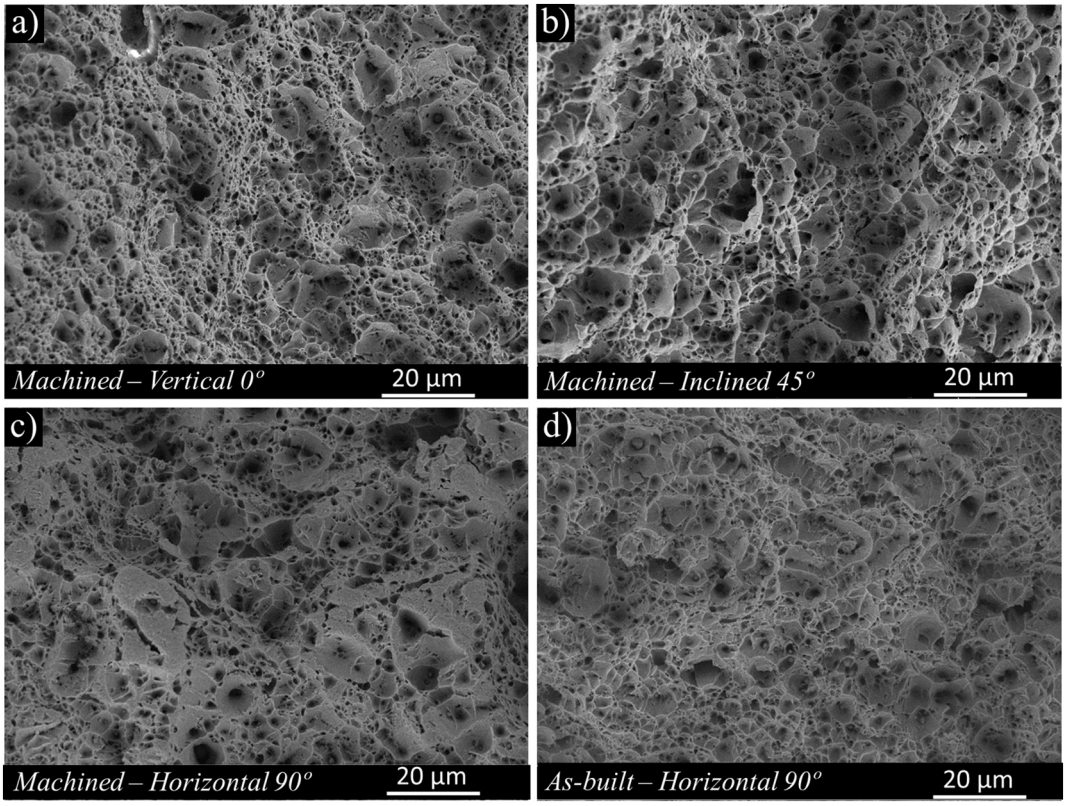

Fig. 10. Micrographs of the fibrous region (central region of the fracture surfaces): (a) vertical, machined condition; (b) inclined, machined condition; (c) horizontal, as-machined condition; (d) horizontal, as-built condition.

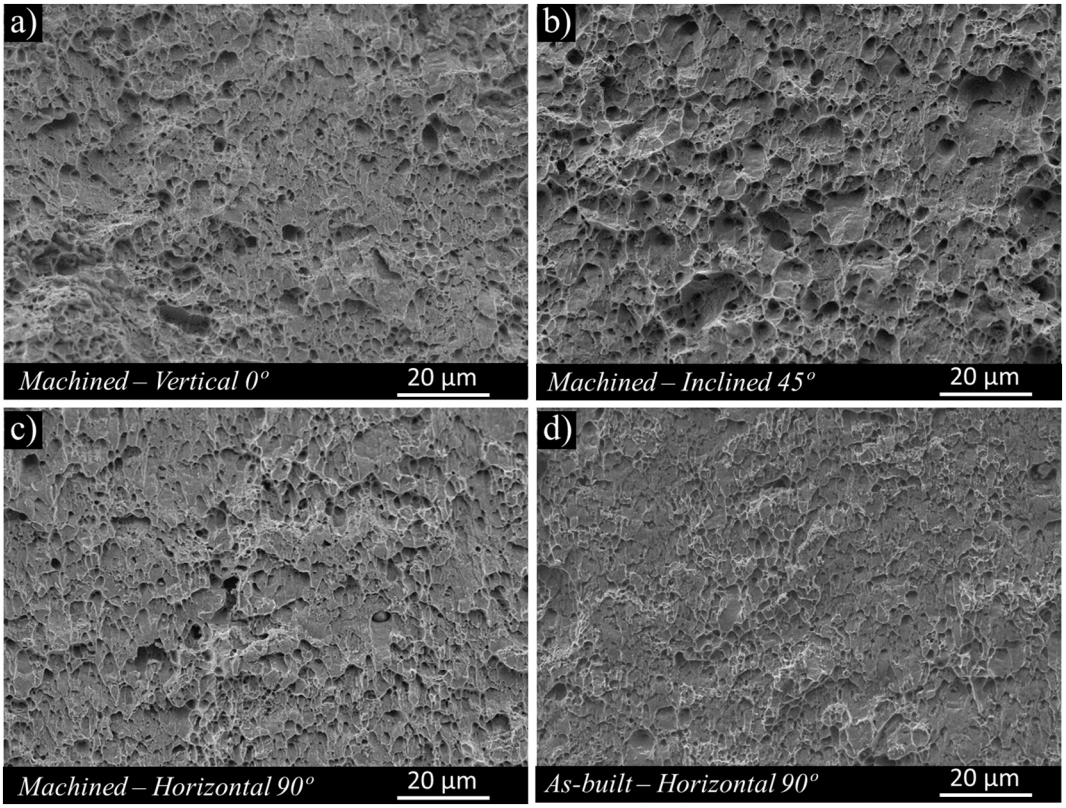

Fig. 11. Micrographs of the smoother region surrounding the fibrous region: (a) vertical, machined condition; (b) inclined, machined condition; (c) horizontal, machined condition; (d) horizontal, as-built condition.

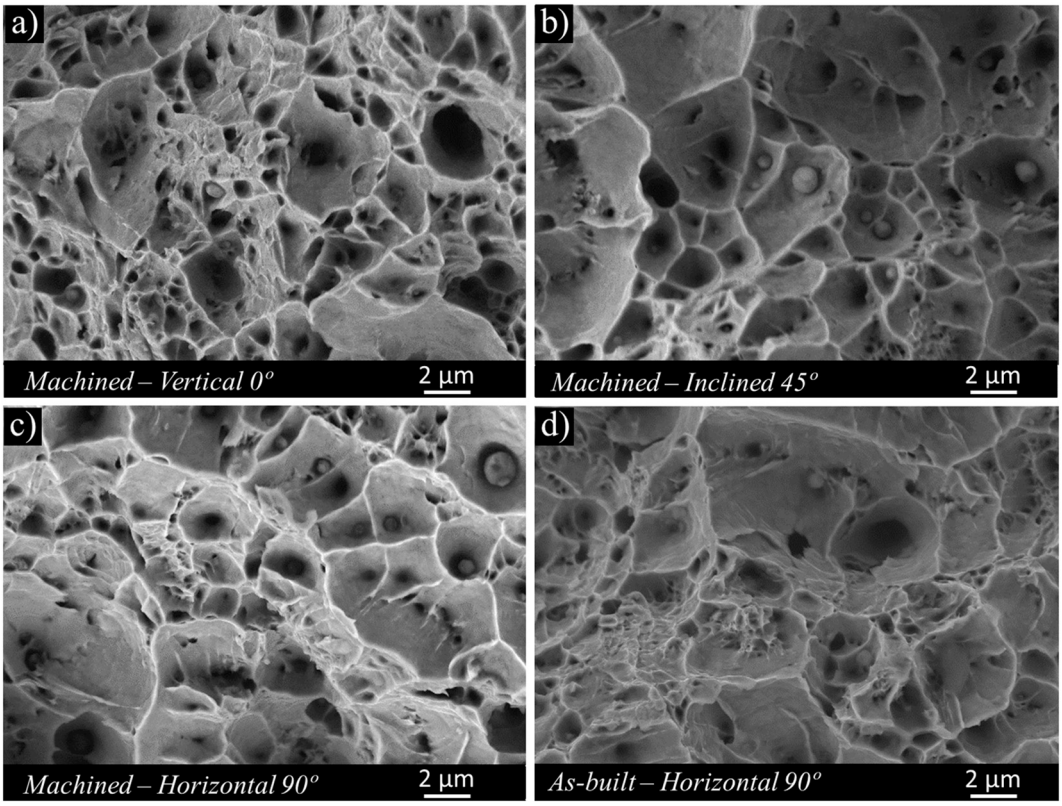

Fig. 12. High-magnification micrographs of the fibrous region (central region of the fracture surfaces): (a) vertical, as-machined condition; (b) inclined, as-machined condition; (c) horizontal, as-machined condition; (d) horizontal, as-built condition.

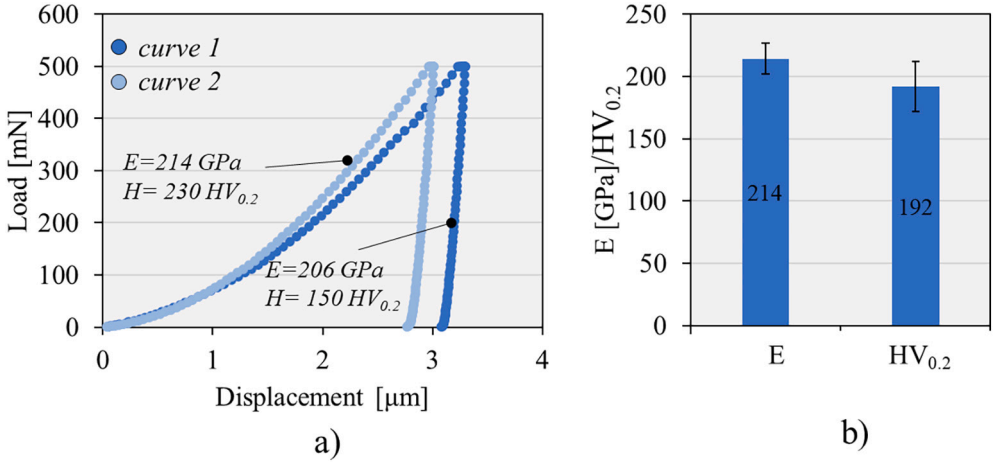

Fig. 13. (a) Depth-sensing indentation load-displacement curves registered at different wall locations and (b) average, maximum and minimum material Young's modulus and hardness.

more detailed analysis of the HAZ enabled to identify the presence of a partially transformed zone (Fig. 14 f), a recrystallised zone (Fig. 14 e) and a coarse grained zone (Fig. 14 d). Since the components produced by WAAM are built layer by layer, the heat input generated by each pass leads to partial remelting of the previous ones, and the multilayer structure of the substrate HAZ is not present in the wall. Due to the low carbon content of the feedstock wire, with the increase in the vertical distance to the substrate, it is possible to observe that the microstructure of the wall consists of polygonal ferrite and intergranular lamellar pearlite (Fig. 14 d).

Furthermore, in WAAM components, it is typical to observe an increase in the grain size along the build direction due to the heat accumulation at the top deposited layers and due to the substrate heatsink effect [17,21,34]. This may be observed in the middle zone micrographs (Fig. 14 h and i), where it is also possible to observe a microstructure with polygonal ferrite and intergranular lamellar pearlite, with a larger grain size than that shown in Fig. 14 d. The grain size gradient may only be observed in a narrow region close to the substrate. Since the thermal cycle history experienced by the deposited material along the build direction reached steady-state conditions, the formation of almost constant microstructure was achieved. Finally, typical layered/heterogeneous microstructure formed by a mixture of polygonal ferrite, acicular ferrite and bainite that was reported by several authors in carbon steel walls [14]–[17] was not observed in the

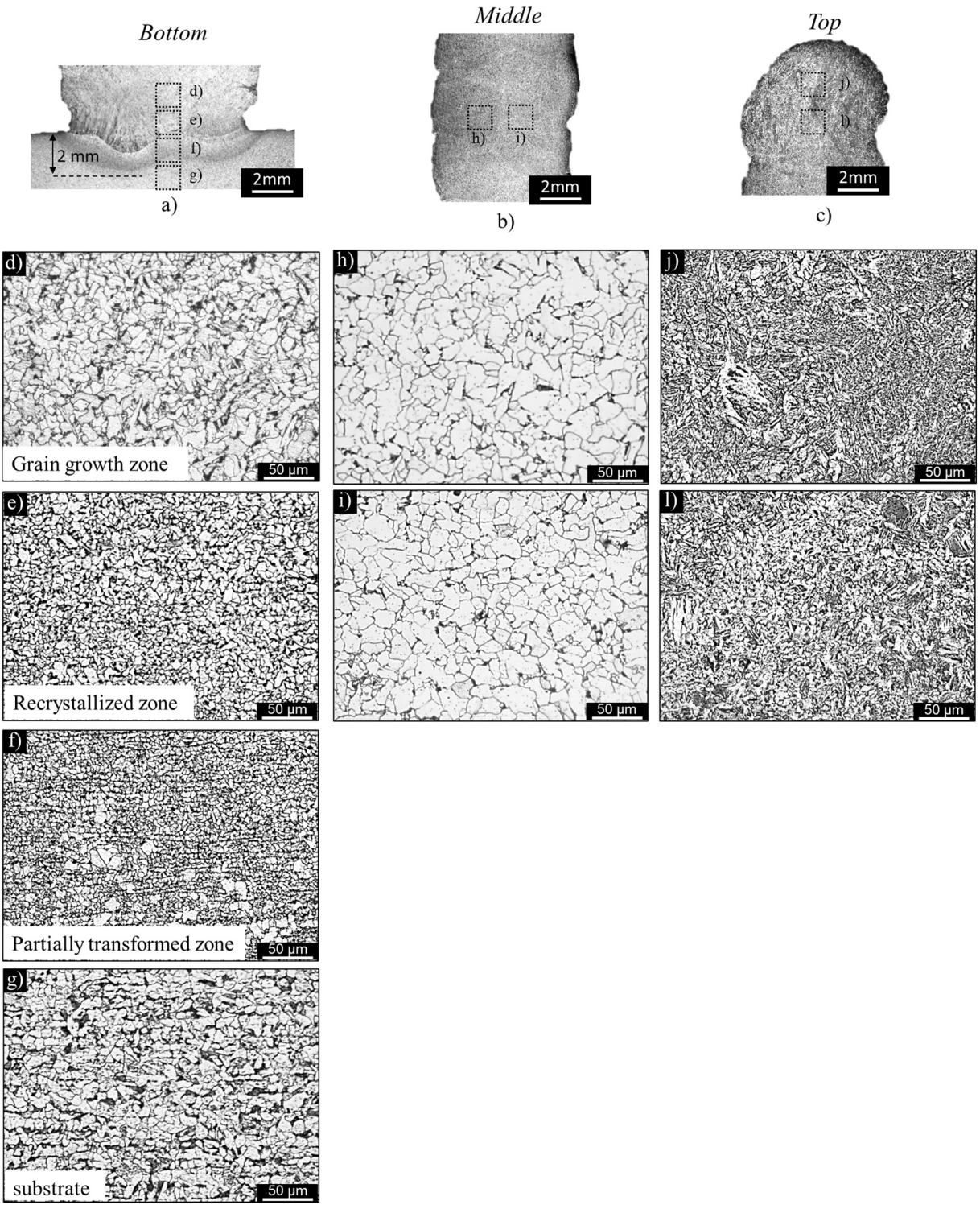

Fig. 14. Micrographs of the wall at the (a, d to g) bottom, (b, h and i) middle and (c,j and l) top regions.

present study. This fact is related to the manufacturing procedures adopted in the current work, which determined not only the complete recrystallisation of the previously deposited microstructures, but also an important grain growth in the recrystalized layers during the building of the wall.

As shown in Fig. 14 j and l, only the last layers of the wall showed a microstructure different from that of the middle layers of the wall. As shown in the figure, the top layers were composed of a mixture of acicular ferrite and bainite microstructures, which is known to provide a good combination of strength and toughness [35], when the electrode used as feedstock in the current work is used in welding. No polygonal ferrite is observed in the images, since this region was not subjected to the thermal effect of the successively deposited layers, which resulted in faster cooling rates. A similar microstructure in the last deposited layers was also reported in several studies of ER70S-6 WAAM fabricated walls [14–17,21].

To assess any possible anisotropy in the microstructure of the wall a more detailed analysis of the grain morphology in the middle region of

the wall was performed. Fig. 15 combines three orthogonal micrographs along the LD, TD and ND directions. More precisely, Fig. 15 a, b and c show results of the microstructure, the phase and the grain size analysis, respectively. Fig. 15 a shows the same microstructure composed of polygonal ferrite and intergranular lamellar pearlite, for all the LD, TD and ND directions, which proves that the microstructure is effectively homogeneous and isotropic across the wall, except in the outer layers. To quantify the volume fraction of the pearlite phase formed along the LD, TD and ND directions, image analysing software was used for producing the images shown in Fig. 15 b, in which the pearlite phase is enhanced by using a red colour. The figure shows that the volume fraction of the pearlite phase was approximately equal to 3.1%, 3.4% and 4.2% on the ND-TD, LD-ND and LD-TD planes, respectively, which is in accordance with the wire chemical composition (Table 2).

Finally, the grain size evolution is represented in Fig. 15 c. The grain size measurements were also conducted using an image analysing software on the micrographs of Fig. 15 a, to create grain size distribution maps. In addition, Fig. 16 a and b show the grain size distribution obtained from the grain size maps from Fig. 15 c, and the grain size average and standard deviation values measured in three different locations, respectively, along the ND-TD, LD-ND and LD-TD planes. The figures enable to observe that, independently of the wall direction, the grain size distribution was identical in all printing planes. Furthermore, the average grain size was uniform along the wall, varying from a minimum value of 9 μm to a maximum value of 13 μm. The results shown in Fig. 15 and Fig. 16 are also in good agreement with the wall's mechanical properties, which were constant irrespective of the printing direction.

4. Conclusions

This paper analysed the microstructural and mechanical properties of carbon steel specimens produced by WAAM using the CMT technique. The analyses covered tensile coupon tests and examination of fracture surfaces by SEM for machined and as-built specimens; hardness study

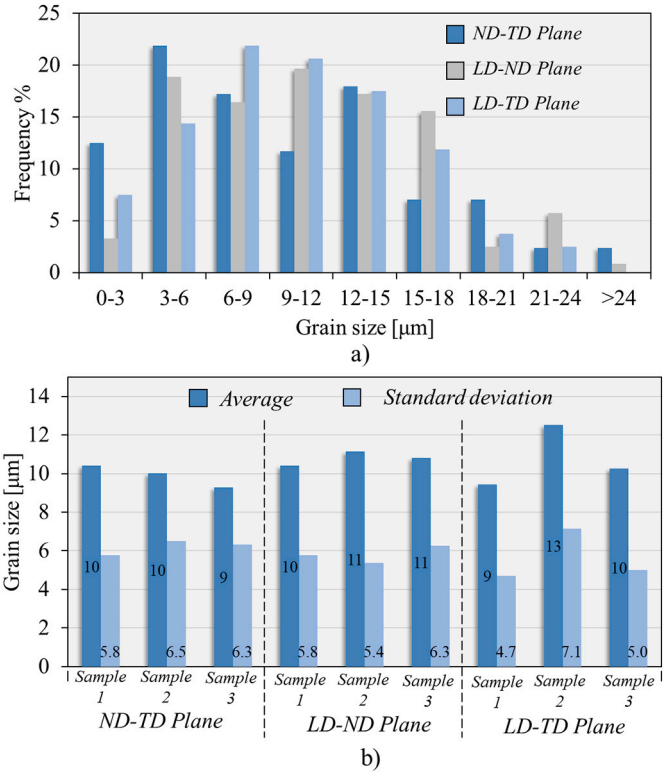

Fig. 16. (a) Grain size distribution and (b) grain size average and standard deviation values.

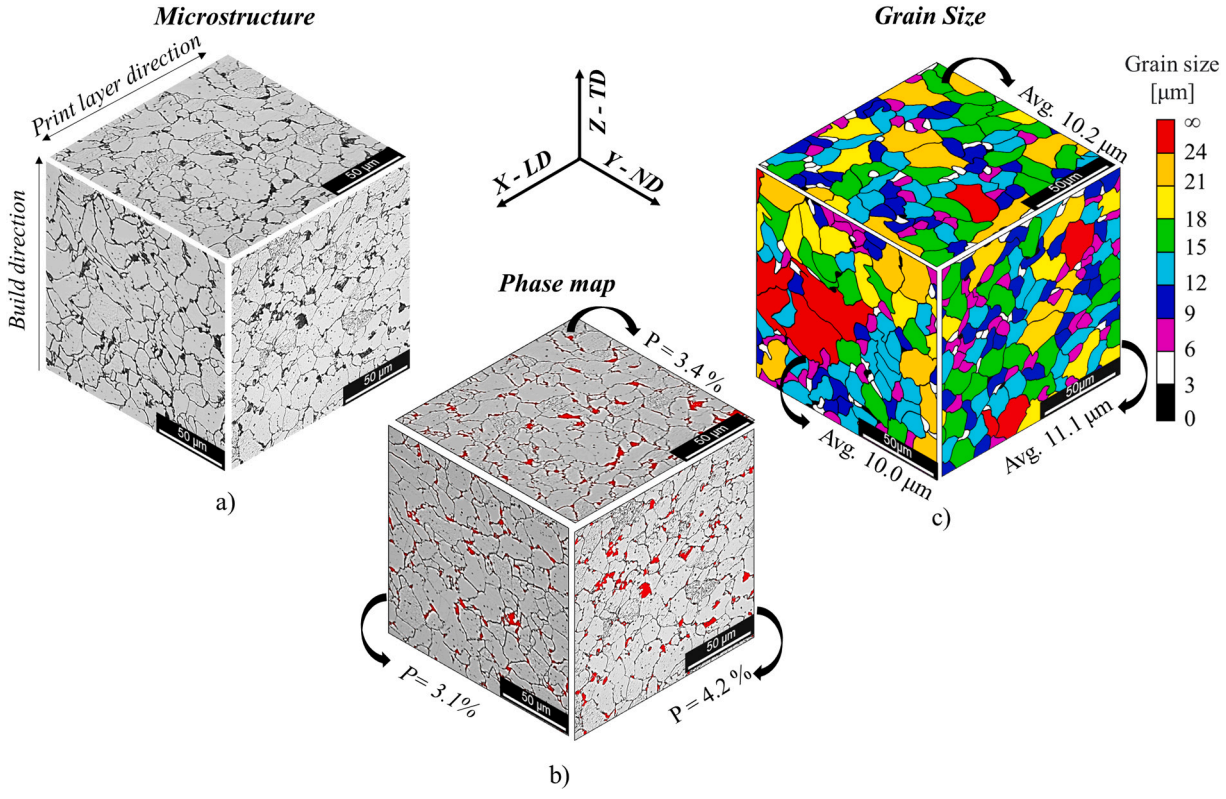

Fig. 15. Isometric micrographs of metallographic samples: (a) microstructural analysis, (b) phase analysis and (c) grain size analysis.

and deep microstructural characterization. Based on the analyses performed, the following conclusions were drawn:

- In general, the machined coupons exhibited higher strength and ductility in all tests.
- The yield stress and tensile strength of machined coupons did not vary with the printing direction, which was not the case for the as-built coupons, which was attributed to the variation of the surface roughness and the presence of surface defects.
- The ductility requirements according to EN 1993-1-1 [3] were satisfied for both machined and as-built coupons. Regarding the strength of the coupons, the machined coupons showed good correlation with the mechanical properties of the feedstock material, that satisfied the minimum requirements for S355 [3]. The as-built samples exhibited lower values for f_y and f_u but, from a structural point of view, a possible approach to design steel structures with as-built components is to adopt the mechanical properties of the machined steel combined with an appropriate effective thickness.
- The wall microstructure exhibits three different distinctive regions: a lower region close to the subtract exhibited a partially transformed zone, a recrystallised zone and a coarse-grained zone; the middle region, which was the most predominant region across the wall, featured a microstructure with polygonal ferrite and intergranular lamellar pearlite; and the upper region showed a mixture of acicular ferrite and bainite microstructures.
- Fracture surfaces of both the as-built and the machined conditions for the three tested directions (vertical, inclined, and horizontal) exhibited a ductile behaviour and a large amount of plastic deformation. The machined condition resulted in a more ductile behaviour than the as-built condition.
- The morphology of the fracture surfaces for all cases was characterized by two distinct regions: a more fibrous region in the centre of the samples, surrounded by a smoother region with 45° shear lips in the edges.
- The size and shape of the dimples varied with the printing direction and these features were related with the ductility. The dimples were more regularly distributed and had a more uniform size for the inclined samples than those of the other directions.

Finally, the relation of the material properties to the fabrication procedure is the key for establishing quality parts using metal additive manufacturing. Nevertheless, it is worth to note that despite the WAAM technology used in this research - a robotized Fronius CMT system - and the processing parameters selected to produce the carbon steel parts were different from those studied in the open literature, the mechanical properties were quite similar, as demonstrates the comparative analysis carried out in the previous section. To generalize this interdependency as well as to develop a parameter-microstructure-property database, it is necessary to perform more studies in a systematic way.

CRediT authorship contribution statement

Trayana Tankova: Validation, Methodology, Supervision, Conceptualization, Writing – original draft, Writing – review & editing, Funding acquisition. **David Andrade:** Investigation, Writing – original draft, Writing – review & editing. **Ricardo Branco:** Investigation, Validation, Methodology, Writing – original draft, Writing – review & editing. **Carlos Zhu:** Investigation, Writing – review & editing. **Dulce Rodrigues:** Validation, Methodology, Supervision, Conceptualization, Writing – original draft, Writing – review & editing. **Luís Simões da Silva:** Validation, Supervision, Conceptualization, Writing – review & editing.

Declaration of Competing Interest

All the authors that there is no conflict of interest.

Data availability

The data that is not explicitly given in the tables of the paper is confidential until the conclusion of the PhD thesis of Carlos Zhu.

Acknowledgments / Funding

This work was partly financed by:

i) FCT / MCTES through national funds (PIDDAC) under the R&D Unit Institute for Sustainability and Innovation in Engineering Structures (ISISE), under reference UIDB / 04029/2020
ii) CEMMPRE: This research is sponsored by FEDER funds through the program COMPETE – Programa Operacional Factores de Competitividade – and by national funds through FCT – Fundação para a Ciência e a Tecnologia – under the projects UIDB/00285/2020.
iii) FCT grant with reference 2021.05992.BD attributed to the fourth author.
iv) The AMCONSTRUCTION project, which is part of the UC PATRONAGE 2019 initiative and a joint effort between CEMMPRE (R&D Unit, The Centre for Mechanical Engineering, Materials and Processes) and ISISE (R&D Unit Institute for Sustainability and Innovation in Structural Engineering)

References

[1] CEN, European Committee for Standardization, EN 10025: 2004 – Hot Rolled Products of Structural Steels, 2004.
[2] CEN, EN 1990, Eurocode – Basis of Structural Design, CEN, Brussels, 2002.
[3] CEN, EN 1993-1-1, Eurocode 3: Design of Steel Structures - Part 1–1: General Rules and Rules for Buildings, CEN, Brussels, 2005.
[4] A. Gisario, M. Kazarian, F. Martina, M. Mehrpouya, Metal additive manufacturing in the commercial aviation industry: a review, J. Manuf. Syst. 53 (2019) 124–149.
[5] C. Buchanan, V.P. Matilainen, A. Salminen, L. Garnder, Structural performance of additive manufactured metallic material and cross-sections, J. Constr. Steel Res. 136 (2017) 35–48.
[6] J.P. Oliveira, T.G. Santos, R.M. Miranda, Revisiting fundamental welding concepts to improve additive manufacturing: from theory to practice, Prog. Mater. Sci. 107 (2020), 100590.
[7] Y. Zhang, A. Bernard, R. Harik, K.P. Karunakaran, Build orientation optimisation for multi-part production in additive manufacturing, J. Intell. Manuf. 28 (2017) 1393–1407.
[8] E. Sabourin, S.A. Houser, J.H. Bohn, Adaptive slicing using stepwise uniform refinement, Rapid Prototyp. J. 2 (1996) 20–26.
[9] T.A. Rodrigues, V. Duarte, R.M. Miranda, T.G. Santos, J.P. Oliveira, Current status and perspectives on wire and arc additive manufacturing (WAAM), Materials 12 (2019) 1121.
[10] J.N. Pires, A.S. Azar, F. Nogueira, C. Zhu, R. Branco, T. Tankova, The role of robotics in additive manufacturing: review of the am processes and introduction of an intelligent system, Ind. Robot. 49 (2022) 311–331.
[11] ISO, ISO 6892–1:2009. Metallic materials – Tensile Testing – Part 1: Method of Test at Room Temperature, International Organization for Standardization, 2009.
[12] W.C. Oliver, G.M. Pharr, Measurement of hardness and elastic modulus by instrumented indentation: advances in understanding and refinements to methodology, J. Mater. Res. 19 (2004) 3–20.
[13] V.S. Ananthan, E.O. Hall, Macroscopic aspects of Lüders band deformation in mild steel, Acta Metall. Mater. 39 (1991) 3153–3160.
[14] B.P. Nagasai, S. Malarvizhi, V. Balasubramanian, Effect of welding processes on mechanical and metallurgical characteristics of carbon steel cylindrical components made by wire arc additive manufacturing (WAAM) technique, CIRP J. Manuf. Sci. Technol. 36 (2022) 100–116.
[15] M. Rafieazad, M. Ghaffari, Nemani A. Vahedi, A. Nasiri, Microstructural evolution and mechanical properties of a low-carbon low-alloy steel produced by wire arc additive manufacturing, Int. J. Adv. Manuf. Technol. 105 (2019) 2121–2134.
[16] V.T. Le, D.S. Mai, Q.H. Hoang, A study on wire and arc additive manufacturing of low-carbon steel components: process stability, microstructural and mechanical properties, J. Braz. Soc. Mech. Sci. Eng. 42 (2020) 1–11.
[17] E. Aldalur, F. Veiga, A. Suárez, J. Bilbao, A. Lamikiz, High deposition wire arc additive manufacturing of mild steel: strategies and heat input effect on microstructure and mechanical properties, J. Manuf. Process. 58 (2020) 615–626.
[18] Y. Ayan, N. Kahraman, Wire arc additive manufacturing of low-carbon mild steel using two different 3D printers, Phys. Met. Metallogr. (2021) 2021.
[19] A. Astarita, G. Campatelli, P. Corigliano, G. Epasto, F. Montevecchi, F. Scherillo, G. Venturini, Microstructure and mechanical properties of specimens produced

using the wire-arc additive manufacturing process, Proc. Inst. Mech. Eng. Part C J. Mech. Eng. Sci. 235 (2021) 1788–1798.
[20] H. Xin, I. Tarus, L. Cheng, M. Veljkovic, N. Persem, L. Lorich, Experiments and numerical simulation of wire and arc additive manufactured steel materials, Structures. 34 (2021) 1393–1402.
[21] C. Huang, P. Kyvelou, R. Zhang, Britton T. Ben, L. Gardner, Mechanical testing and microstructural analysis of wire arc additively manufactured steels, Mater. Des. 216 (2022), 110544.
[22] Z. Al-Nabulsi, J.T. Mottram, M. Gillie, N. Kourra, M.A. Williams, Mechanical and X ray computed tomography characterisation of a WAAM 3D printed steel plate for structural engineering applications, Constr. Build. Mater. 274 (2021), 121700.
[23] V.A. Silvestru, I. Ariza, J. Vienne, L. Michel, A.M. Aguilar Sanchez, U. Angst, R. Rust, F. Gramazio, M. Kohler, A. Taras, Performance under tensile loading of point-by-point wire and arc additively manufactured steel bars for structural components, Mater. Des. 205 (2021), 109740, https://doi.org/10.1016/j.matdes.2021.109740.
[24] M. Liberini, A. Astarita, G. Campatelli, A. Scippa, F. Montevecchi, G. Venturini, Selection of optimal process parameters for wire arc additive manufacturing, Procedia CIRP 62 (2017) 70–474.
[25] N. Sridharan, M.W. Noakes, A. Nycz, L.J. Love, R.R. Dehoff, S.S. Babu, On the toughness scatter in low alloy C-Mn steel samples fabricated using wire arc additive manufacturing, Mater. Sci. Eng. A 713 (2018) 8–27.
[26] A. Ermakova, A. Mehmanparast, S. Ganguly, J. Razavi, F. Berto, Investigation of mechanical and fracture properties of wire and arc additively manufactured low carbon steel components, Theor. Appl. Fract. Mech. 109 (2020), 102685.
[27] C.V. Haden, G. Zeng, F.M. Carter, C. Ruhl, B.A. Krick, D.G. Harlow, Wire and arc additive manufactured steel: tensile and wear properties, Addit Manuf 16 (2017) 115–138.
[28] J.L. Prado-Cerqueira, A.M. Camacho, J.L. Diéguez, Á. Rodríguez-Prieto, A. M. Aragón, C. Lorenzo-Martín, Analysis of favorable process conditions for the manufacturing of thin-wall pieces of mild steel obtained by wire and arc additive manufacturing (WAAM), Materials (Basel) (2018) 11.
[29] A. Scotti, V. Ponomarev, W. Lucas, A scientific application oriented classification for metal transfer modes in GMA welding, J. Mater. Process. Technol. 212 (2012) 1406–1413.
[30] A. Scotti, V. Ponomarev, W. Lucas, Interchangeable metal transfer phenomenon in GMA welding: features, mechanisms, classification, J. Mater. Process. Technol. 214 (2014) 2488–2496.
[31] Elias Oliveira Romualdo da Silva, Fabrico Aditivo para a Construção Metálica: Projeto, Realização e Caracterização, Mestrado Integrado em Engenharia Civil, 2021.
[32] X. Chen, J. Li, X. Cheng, B. He, H. Wang, Z. Huang, Microstructure and mechanical properties of the austenitic stainless steel 316L fabricated by gas metal arc additive manufacturing, Mater. Sci. Eng. A 703 (2017) 567–577.
[33] E.J. Pavlina, C.J. Van Tyne, Correlation of Yield Strength and Tensile Strength with Hardness for Steels, 2008, p. 17.
[34] Z. Lin, C. Goulas, W. Ya, M.J.M. Hermans, Microstructure and mechanical properties of medium carbon steel deposits obtained via wire and arc additive manufacturing using metal-cored wire, Metals (Basel) (2019) 9.
[35] S.S. Babu, The mechanism of acicular ferrite in weld deposits, Curr. Opin. Solid State Mater. Sci. 8 (2004) (2004) 267–278.